Journal of Medicinal Chemistry

Article

pubs.acs.org/jmc

Purification-Free Method for Preparing Technetium-99m-Labeled Multivalent Probes for Enhanced in Vivo Imaging of Saturable Systems

Yuki Mizuno,[†,‡] Tomoya Uehara,[†] Hirofumi Hanaoka,[†,§] Yota Endo,[†] Chun-Wei Jen,[†] and Yasushi Arano*[,†]

[†]Department of Molecular Imaging and Radiotherapy, Graduate School of Pharmaceutical Sciences, Chiba University, 1-8-1 Inohana, Chuo-ku, Chiba 260-8675 Japan

[‡]Research Fellow of Japan Society for the Promotion of Science and [§]Department of Bioimaging Information Analysis, Graduate School of Medicine, Gunma University, 3-39-15 Showa-chou, Maebashi 371-8511 Japan

Supporting Information

ABSTRACT: Metallic radionuclides provide target-specific radiolabeled probes for molecular imaging in radiochemical yields sufficient for administration to subjects without purification. However, unlabeled ligands in the injectate can compete for targeted molecules with radiolabeled probes, which eventually necessitates postlabeling purification. Herein we describe a "1 to 3" design to circumvent the issue by taking advantage of inherent coordination properties of technetium-99m (^{99m}Tc). A monovalent RGD ligand possessing an isonitrile as a coordinating moiety (CN-RGD) was reacted with $[^{99m}Tc(CO)_3(OH_2)_3]^+$ to prepare $[^{99m}Tc(CO)_3(CN\text{-}RGD)_3]^+$ in over 95% radiochemical yields. This complex exhibited higher integrin $\alpha_v\beta_3$ binding affinity than its unlabeled monovalent ligand, primarily due to its multivalency. This compound visualized a murine tumor without removing unlabeled ligands, while a ^{99m}Tc-labeled monovalent probe derived from a monovalent ligand could not. The metal coordination-mediated synthesis of radiolabeled multivalent probes thereby can be a useful approach for preparing ready-to-use target-specific probes labeled with ^{99m}Tc and other metallic radionuclides of interest.

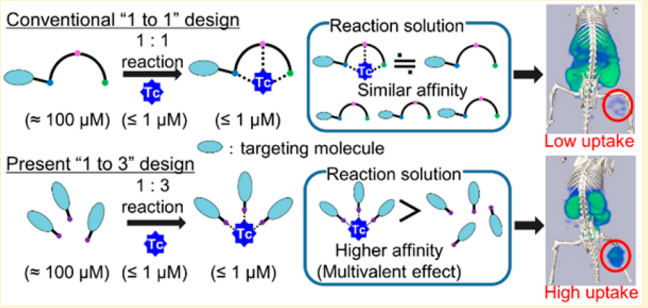

INTRODUCTION

Radiolabeled molecular imaging probes have now become a powerful tool for noninvasive monitoring of biological processes at the cellular and/or molecular level.[1−5] In these radiolabeled probes, targeting vectors possessing high affinities to specific biological targets are conjugated with gamma (γ) or positron (β^+) emitting radionuclides suitable for single photon emission computed tomography (SPECT) or positron emission tomography (PET) imaging, respectively. Among the radionuclides, metallic radionuclides such as technetium-99m (^{99m}Tc), gallium-67/68, and indium-111 have an advantage over nonmetallic radionuclides such as carbon-11 and fluorine-18, as these metallic radionuclides are available via a generator system and/or can provide objective radiolabeled probes in radiochemical yields sufficient for administration to subjects without purification.[6−11] Indeed, most radiometal-labeled probes used in clinical practice today are prepared in >95% radiochemical yields and administered to patients without any purification steps, which allows widespread applications of the radiometal-labeled probes for molecular imaging.

The synthesis of radiometal-labeled probes is a competitive reaction between complexation with a chelators-vector conjugate (hereafter referred as "ligand") and hydrolysis of the radiometal at extremely low radiometal concentrations (for example ^{99m}Tc ≤ 1 μM).[10] Therefore, a large excess of ligand over metallic radionuclide is used to ensure high radiochemical yields in short reaction times. As a result, the reaction solution contains an excess of unlabeled ligands along with the objective radiometal-labeled probes (Figure 1).

Most metallic radiopharmaceuticals currently used in clinical settings are designed to image large capacity nonsaturable systems such as bone, glomerular filtration, cerebral, or myocardial perfusion, and the presence of unlabeled ligand in the injectate does not affect the target localization of these probes.[12] When imaging saturable systems in the brain such as neuronal receptors or transporters, the presence of unlabeled ligand does not compete since the radiolabeled probes are designed to achieve much higher penetration through the blood-brain-barrier than their unlabeled charged ligands.[13] However, when designing radiolabeled probes for saturable systems in the peripheral tissues, the presence of unlabeled ligand can compete with the radiolabeled probe for the targeted

Received: January 7, 2016

DOI: 10.1021/acs.jmedchem.6b00024
J. Med. Chem. XXXX, XXX, XXX−XXX

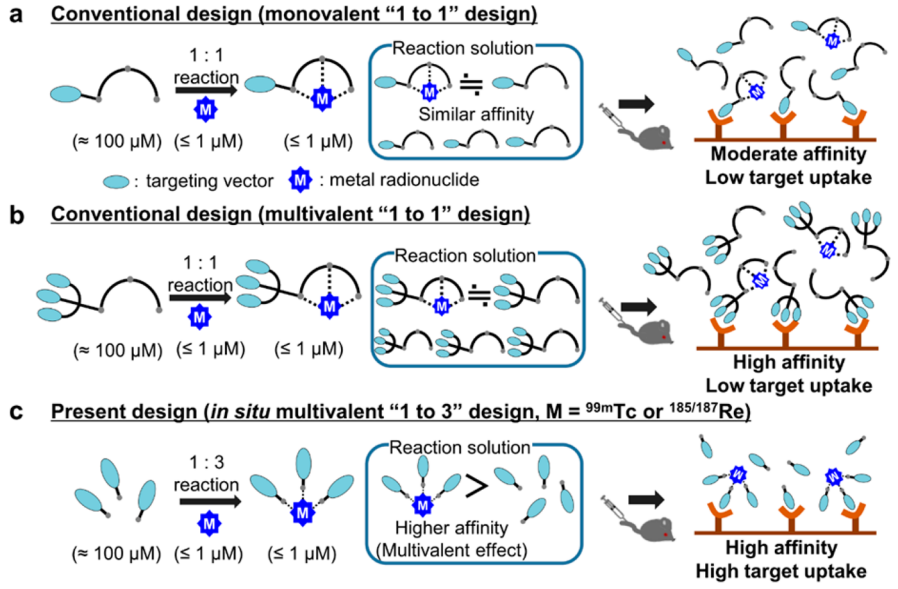

Figure 1. A conceptual illustration of the three different molecular design strategies. (a) In a monovalent "1 to 1" design, both an unlabeled ligand and a final radiolabeled probe possess the same monovalent targeting vector and display similar binding affinities to a target molecule. Upon in vivo injection, the presence of the unlabeled ligand reduces the in vivo target uptake of the radiolabeled probe due to the competitive inhibition by the unlabeled ligand. (b) In a multivalent "1 to 1" design, both a radiolabeled probe and an unlabeled ligand display higher binding affinities to a target molecule due to the multivalent effect. The improved in vivo targeting of the radiolabeled probe is diminished in vivo due to the presence of the high affinity unlabeled ligand in the injectate, resulting in the lower accumulation of the radiolabeled probe at the target. (c) In the in situ multivalent "1 to 3" design, an unlabeled monovalent ligand upon metal complexation results in a multivalent radiolabeled probe that has acquired in situ trivalency of a targeting vector and displays higher binding affinity than its unlabeled monovalent construct. This "acquired" multivalency of the radio-labeled probe results in higher affinity for the target and reduces the competitive inhibition from the unlabeled ligand, thus displaying enhanced in vivo target localization.

molecule and significantly decreases the accumulation of the radiolabeled probes at the target site. This is primarily due to the presence of much higher amount of the unlabeled ligand and similar binding affinity between the radiometal-labeled probe and the unlabeled ligand[14,15] (Figure 1a,b). This competitive inhibition can be eliminated by a postlabeling removal of the unlabeled ligands by HPLC or other purification procedures. However, these additional steps significantly impair the practical utility and advantages of the metallic radionuclides.[14]

To address the issue, we envisioned a novel molecular design using the unique behavior of metals to serve as a template for coordinating multiple monovalent ligands (Figure 1c). Since multivalent probes possessing multivalent targeting moieties on a molecule exhibit higher binding affinities to the target than their monovalent counterparts,[16,17] the resulting multivalent probes would decrease the level of competitive inhibition at the target in the presence of unlabeled monovalent ligand. To examine the validity of this in situ multivalent approach, we applied the concept to the radiometal technetium-99m (^{99m}Tc), the most widely available and frequently used radiometal in diagnostic nuclear medicine. We then chose an isonitrile (CN-R)−$[^{99m}Tc(CO)_3]^+$ core combination as a model, because an isonitrile group strongly coordinates the $[^{99m}Tc(CO)_3]^+$ core in a monodentate fashion with a metal to chelator ratio of 1:3.[18−20] The cyclic RGDfK (-Arg-Gly-Asp-D-Phe-Lys-; cRGDfK) peptide, a specific antagonist for integrin $\alpha_v\beta_3$[21] was also selected as a model of a specific targeting vector. The c(RGDfK) peptide was conjugated to the carboxyl residue of terminal isonitrile β-Ala-Gly-Gly peptide to synthesize the monovalent targeting ligand CN-β-Ala-Gly-Gly-c(RGDfK) (Figure 2, L2) and its ^{99m}Tc-labeled trivalent complex, $[^{99m}Tc(CO)_3(L2)_3]^+$ (Figure 2, ^{99m}Tc-$[L2]_3$). We introduced the Gly-Gly spacer at each RGD motif to provide the recommended distance between the targeting vector position[22,23] and to enhance the hydrophilicity of the molecule. To comparatively assess the in situ multivalent "1 to 3" design

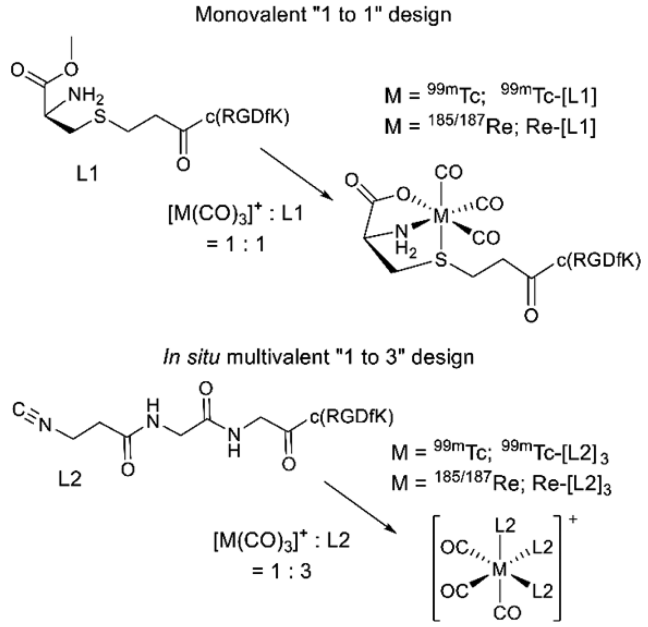

Figure 2. Chemical structures of L1 (monovalent "1 to 1" design), L2 (in situ multivalent "1 to 3" design), and their metal complexes. Both L1 and L2 act as monovalent ligands. Upon metal complexation, L1 generates a monovalent radiolabeled probe, M-[L1], while L2 results in a trivalent radiolabeled probe, M-$[L2]_3$.

DOI: 10.1021/acs.jmedchem.6b00024
J. Med. Chem. XXXX, XXX, XXX−XXX

Scheme 1. Synthesis of L2[a]

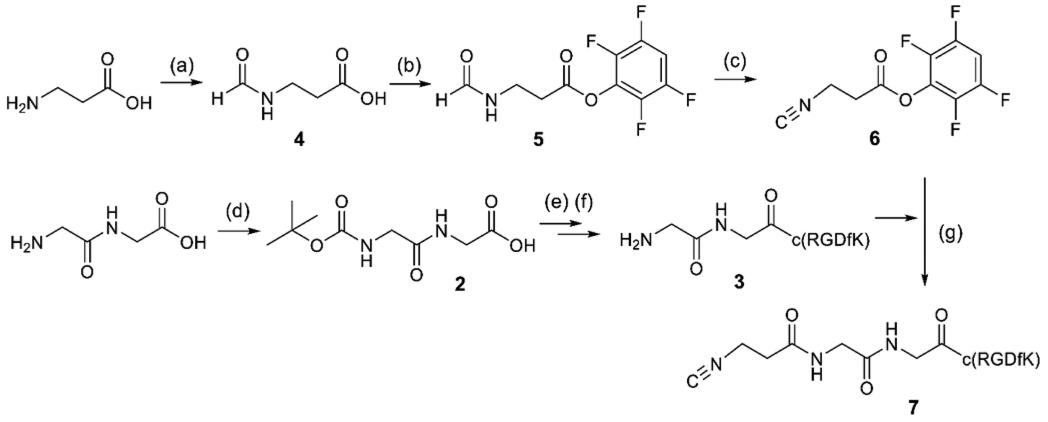

[a]Reagents and conditions: (a) formic acid, acetic anhydrate, 60%; (b) 2,3,5,6-tetrafluorophenol, DCC, DMF, 53%; (c) Burgess reagent, CH_2Cl_2, 83%; (d) di-*tert*-butyl dicarbonate, water, dioxane, 1 N $NaOH_{aq}$, 42%; (e) c[R(pbf)GD(*t*Bu)fK], DIC, HOBt, DMF; (f) TFA, TES, water, 59% over steps e–f; (g) DIPEA, DMF, 49%.

(Figure 1c) against the conventional monovalent "1 to 1" design methods (Figure 1a), the c(RGDfK) peptide was separately conjugated with a cysteine derivative, which is known to form a stable complex with $[^{99m}Tc(CO)_3]^+$ core in a 1:1 molar ratio[24] (Figure 2, L1).

RESULTS

Synthesis. The synthesis of the isocyanide-conjugated c(RGDfK) (L2) is illustrated in Scheme 1. First, β-alanine (β-Ala) was N-formylated, and its carboxylic acid was converted to 2,3,5,6-tetrafluorophenol (TFP) ester. The formyl-β-Ala-TFP was then treated with burgess reagent[25] to provide isocyano-β-Ala-TFP. This isocyanide-containing active ester was conjugated with H_2N-Gly-Gly-c(RGDfK) peptide where the Gly-Gly spacer is introduced at the ε-amine residue of Lys (K) in the peptide. The peptide construct CN-βAla-GlyGly-c(RGDfK) was subsequently purified via preparative HPLC.

^{99m}Tc-Labeled Probes. The precursor complex $[^{99m}Tc(OH_2)_3(CO)_3]^+$ was prepared in >95% yields as described previously[26] with slight modification (see Experimental Section). The ^{99m}Tc-[L1] and ^{99m}Tc-$[L2]_3$ complexes were prepared by mixing a L1 or L2 solution with freshly prepared $[^{99m}Tc(OH_2)_3(CO)_3]^+$, followed by heating the reaction mixture. The optimized radiolabeling conditions to prepare ^{99m}Tc-$[L2]_3$ were determined to be 150 μM of L2 concentration (40 nmol/265 μL), pH 6.0 at 110 °C for 20 min, followed by 100 °C for 20 min in a heating block. These conditions consistently provided over 95% radiochemical yields of the ^{99m}Tc-$[L2]_3$ complex (Figure 3). Similarly, ^{99m}Tc-[L1] was synthesized over 95% radiochemical yields at pH 6.0, using 50 μM of L1 (20 nmol/400 μL) and heating at 110 °C for 30 min in a heating block. The HPLC retention times of the two ^{99m}Tc complexes were identical to the corresponding macroscopic and nonradioactive Re complexes characterized and verified by ESI-MS separately (Figures 3 and S1).

The log $D_{7.4}$ values of ^{99m}Tc-[L1] and ^{99m}Tc-$[L2]_3$ were −2.16 ± 0.03 and −1.18 ± 0.01, respectively.

Stability Assessment. The high stability of ^{99m}Tc-[L1] in plasma solution has been reported elsewhere,[24] whereas the stability of ^{99m}Tc-$[L2]_3$ was assessed in a 10 mM histidine solution or in murine plasma at 37 °C. Under both conditions, TLC analyses revealed more than 95% of ^{99m}Tc-$[L2]_3$ remained intact after 6 h incubation (Table 1). Additional HPLC analyses performed at 6 h postincubation for both conditions indicated no degradation of ^{99m}Tc-$[L2]_3$ (>99%) (Figure 4a,b). The recovery rate of radioactivity from plasma sample to supernatant solution was 63.5 ± 1.4% (n = 3) upon addition of EtOH and protein precipitation.

Table 1. In Vitro Stability of ^{99m}Tc-$[L2]_3$ in 10 mM Histidine Solution and Murine Plasma[a]

	percent of intact	
time (h)	10 mM histidine	murine plasma
1	96.3 ± 0.9	96.8 ± 0.5
6	96.1 ± 0.9	96.6 ± 0.2

[a]Results are expressed as mean ± SD of three experiments. Percent of intact was determined by TLC analysis.

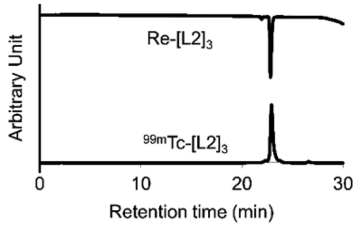

Figure 3. HPLC analysis of ^{99m}Tc-$[L2]_3$ coinjected with Re-$[L2]_3$. The retention time of ^{99m}Tc-$[L2]_3$ was identical to that of Re-$[L2]_3$, which was verified by ESI-MS.

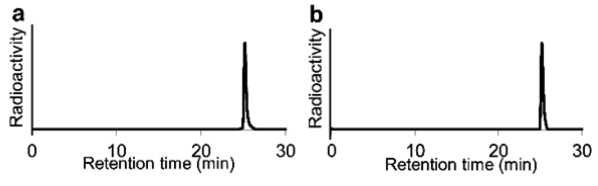

Figure 4. In vitro stability of ^{99m}Tc-$[L2]_3$ in histidine solution and murine plasma. (a) HPLC analysis 6 h postincubation (a) in 10 mM histidine solution and (b) in murine plasma. Plasma proteins were precipitated with EtOH prior to HPLC analysis.

DOI: 10.1021/acs.jmedchem.6b00024
J. Med. Chem. XXXX, XXX, XXX−XXX

Binding Affinity to Integrin $\alpha_v\beta_3$. The integrin $\alpha_v\beta_3$ binding affinities of L1, Re-[L1], L2, Re-$[L2]_3$, and the c(RGDyV) ligand were determined by displacement of ^{125}I-c(RGDyV) bound to integrin $\alpha_v\beta_3$ positive U87MG human glioma cells at 37 °C (Figure 5). The IC_{50} values calculated

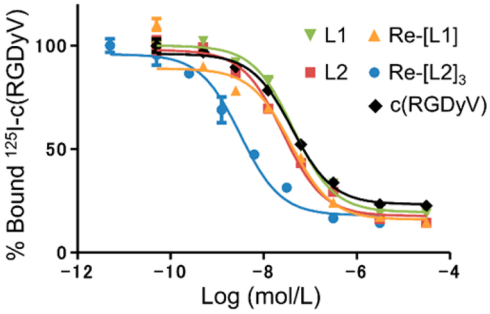

Figure 5. In vitro inhibition curves of ^{125}I-c(RGDyV) bound to U87MG glioma cells by L1, Re-[L1], L2, Re-$[L2]_3$, and c(RGDyV) at 37 °C.

from the displacement curves of ^{125}I-c(RGDyV) are illustrated in Table 2. Both Re-[L1] and L1 showed similar integrin $\alpha_v\beta_3$ receptor affinities, while Re-$[L2]_3$ displayed 8-fold higher binding affinity for integrin $\alpha_v\beta_3$ than its monovalent ligand L2.

Table 2. IC_{50} Values of Each Compound

design	compound	IC_{50}, nM	95% C.I.[a]
"1 to 1"	L1	43.3	34.4–54.5
	Re-[L1]	38.4	28.4–51.9
"1 to 3"	L2	25.9	19.9–33.7
	Re-$[L2]_3$	3.16	2.14–4.68
reference	c(RGDyV)	41.2	34.9–48.7

[a]C.I. = confidential interval.

Biodistribution. The biodistribution of radioactivity at 1 h postadministration in nude mice bearing U87MG xenografts was determined in the following 5 samples: (1) HPLC-purified ^{99m}Tc-$[L2]_3$ (without L2); (2) HPLC-purified ^{99m}Tc-$[L2]_3$ in the presence of 5 nmol Re-$[L2]_3$; (3) unpurified ^{99m}Tc-$[L2]_3$ containing 5 nmol of L2; (4) HPLC-purified ^{99m}Tc-[L1] (without L1); and (5) unpurified ^{99m}Tc-[L1] containing 5 nmol of L1. The results are summarized in Table 3. The tumor accumulation displayed the following order: purified ^{99m}Tc-$[L2]_3$ > unpurified ^{99m}Tc-$[L2]_3$ > purified ^{99m}Tc-[L1] > purified ^{99m}Tc-$[L2]_3$ + Re-$[L2]_3$ > unpurified ^{99m}Tc-[L1]. The tumor uptake of ^{99m}Tc-$[L2]_3$ was significantly reduced in the presence of nonradioactive Re-$[L2]_3$, an illustration of the integrin $\alpha_v\beta_3$ receptor blocking and specificity of ^{99m}Tc-$[L2]_3$ in vivo. Unpurified ^{99m}Tc-$[L2]_3$ displayed significantly higher tumor uptake and tumor to background ratios comparatively not just to unpurified ^{99m}Tc-[L1] but also to purified ^{99m}Tc-[L1], demonstrating the advantage of "1 to 3" design strategy over the conventional "1 to 1" design.

SPECT Imaging. Figure 6 illustrates the SPECT/CT imaging of tumor-bearing mice administered with unpurified

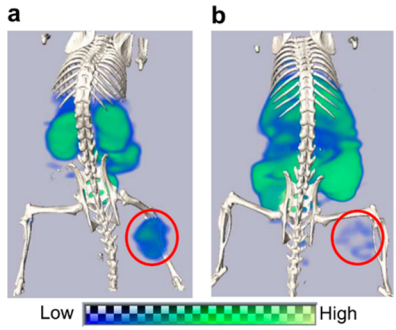

Figure 6. SPECT/CT images of U87MG tumor-bearing male nude mice over 45–75 min post i.v. injection of (a) 7.4 MBq of ^{99m}Tc-$[L2]_3$ coinjected with 5 nmol of L2 and (b) 9.6 MBq of ^{99m}Tc-[L1] coinjected with 5 nmol of L1. Images are shown at the same signal intensity scale. Red circle indicates the U87MG tumor.

^{99m}Tc-$[L2]_3$ (7.4 MBq) containing 5 nmol of L2 (Figure 6a) and a comparative unpurified ^{99m}Tc-[L1] (9.6 MBq) containing 5 nmol of L1 (Figure 6b) over 45–75 min postinjection. Clear visualization of the tumor was demonstrated in the "1 to 3" design (Figure 6a), whereas tumor was barely visualized in the "1 to 1" design (Figure 6b). These images correlated well with the biodistribution results at the similar time point.

Table 3. Biodistribution at 1 h Postinjection in Tumor-Bearing Mice[a]

	^{99m}Tc-$[L2]_3$ ("1 to 3" design)			^{99m}Tc-[L1] ("1 to 1" design)	
	purified	unpurified	purified + Re-$[L2]_3$	purified	unpurified
	L2 = 0 nmol	L2 = 5 nmol	Re-$[L2]_3$ = 5 nmol	L1 = 0 nmol	L1 = 5 nmol
blood	0.30 ± 0.03	0.33 ± 0.08	0.67 ± 0.04	0.50 ± 0.07	0.97 ± 0.10
liver	2.13 ± 0.50	1.38 ± 0.18	1.39 ± 0.14	7.63 ± 1.05	6.83 ± 0.95
kidney	10.91 ± 0.57	10.66 ± 1.29	7.37 ± 0.60	3.84 ± 0.22	3.02 ± 0.48
stomach[b]	0.77 ± 0.07	0.79 ± 0.47	0.64 ± 0.26	0.89 ± 0.39	1.54 ± 1.01
intestine[b]	6.28 ± 0.34	4.27 ± 0.79	4.52 ± 1.38	25.62 ± 3.88	28.52 ± 4.14
muscle	0.73 ± 0.21	0.30 ± 0.04	0.24 ± 0.04	0.30 ± 0.03	0.18 ± 0.05
tumor[c]	7.18 ± 0.60[d]	3.80 ± 0.57	1.80 ± 0.14[d]	2.77 ± 0.51[e]	1.14 ± 0.11[d]
T/blood	24.06 ± 3.89	12.17 ± 4.01	2.70 ± 0.20	5.55 ± 0.48	1.18 ± 0.08
T/liver	3.58 ± 1.10	2.77 ± 0.35	1.31 ± 0.20	0.36 ± 0.06	0.17 ± 0.01
T/muscle	10.37 ± 2.48	12.98 ± 2.80	7.67 ± 1.68	9.12 ± 1.43	6.90 ± 1.60

[a]The results were expressed as percent injected dose per gram (%ID/g) ± SD (n = 5). [b]Expressed as %ID. [c]Statistical analysis was performed using one-way analysis of variance followed by Tukey's multiple-comparison test [d](different from ^{99m}Tc-$[L2]_3$ (L2 = 5 nmol), $p < 0.001$. [e]Different from ^{99m}Tc-$[L2]_3$ (L2 = 5 nmol), $p < 0.05$).

DOI: 10.1021/acs.jmedchem.6b00024
J. Med. Chem. XXXX, XXX, XXX–XXX

DISCUSSION

High and specific in vivo target uptake is a fundamental requirement for molecular-targeted radiolabeled probes to be practical as a molecular imaging tool. Thus, the concept of the multivalent effect has been applied to develop radiolabeled probes of high and specific in vivo targeting abilities, and the effectiveness of this design has been well demonstrated in many targeting vectors such as RGD peptides,[15,22,23,27−29] bombesin,[30] somatostatine,[31] and Lys-Glu urea motif,[32] whose corresponding target molecules are known to overexpress in various pathological conditions.

When a ligand containing multivalent targeting vectors is chelated with a metallic radionuclide of interest (multivalent "1 to 1"; Figure 1b), the radiolabeled probe possesses enhanced binding affinity to the target molecule. However, the unlabeled ligand present in the solution can result in a greater level of in vivo competition at the target site, since both the labeled probe and the unlabeled ligand possess similar binding affinities, which would paradoxically impair the improved binding affinity of the radiolabeled multivalent probe and again compel postlabeling purification steps. Radiolabeling of a monovalent targeting vector (monovalent "1 to 1"; Figure 1a), on the other hand, would display a lower in vivo targeting ability, although the degree of competitive inhibition by the unlabeled ligand observed here would not be as significant as observed in the multivalent "1 to 1" design.

The in situ multivalent "1 to 3" design presented herein (Figure 1c) differs from the two approaches (monovalent and multivalent "1 to 1") as the multivalency itself is induced only upon complexation to the radiometal and not from the uncomplexed ligand, thus preserving the significantly greater binding affinity of the resulting radiolabeled multivalent probe and diminishing the inhibition by the presence of the unlabeled ligand.

Since the quantitative formation of the mixed ligand complex is a prerequisite for the in situ multivalent "1 to 3" design, we initially verified that the model L2 ligand coordinates the $[^{99m}Tc(CO)_3]^+$ metal core with a metal to ligand ratio of 1:3 to form $[^{99m}Tc(CO)_3(L2)_3]^+$ (^{99m}Tc-$[L2]_3$) in high radiochemical yield. To establish the identity of the tracer ^{99m}Tc-$[L2]_3$ complex on macroscopic scale, we also synthesized and characterized the nonradioactive rhenium analogue, since technetium and rhenium share similar coordination chemistry due to their group homology, such that rhenium complexes are routinely used as nonradioactive surrogates of the respective ^{99m}Tc-complexes.[33,34] The HPLC profile in the bottom of Figure 3 shows that heating the reaction mixture of L2 and $[^{99m}Tc(CO)_3(OH_2)_3]^+$ complex produced a single radioactive peak with >95% radiochemical yields. This peak was identified as the objective mixed ligand complex ^{99m}Tc-$[L2]_3$ by comparative HPLC retention time profile with that of rhenium counterpart (Figure 3, Re-$[L2]_3$), indicating that the isonitrile−$[^{99m}Tc(CO)_3]^+$ core combination is an appropriate model platform that induces in situ multivalency of a targeting vector upon complexation reaction. The ligand L1, which is a model ligand for the monovalent "1 to 1" conventional approach, has been previously described[24] and coordinated the $[^{99m}Tc(CO)_3]^+$ core with a metal to ligand ratio of "1:1" to form the $[^{99m}Tc(CO)_3(L1)]$ complex (Figure 2 ^{99m}Tc-[L1], Figure S1).

In vitro stability studies of the mixed ligand complex ^{99m}Tc-$[L2]_3$ were conducted in a physiological ligand (histidine) solution and in murine plasma. More than 95% of ^{99m}Tc-$[L2]_3$ remained intact for 6 h in 10 mM histidine solutions as well as in murine plasma (Table 1, Figure 4a,b), suggesting high in vivo stability of ^{99m}Tc-$[L2]_3$.[35] The high stability of ^{99m}Tc-$[L2]_3$ against a ligand exchange reaction is consistent with the fact that the coordination of an isonitrile to $[^{99m}Tc(CO)_3]^+$ core provides a kinetically inert complex against the substitution due to the strong bonding of an isonitrile toward a low-valent metal center.[36] These chemical features were indeed one of the bases for choosing an isonitrile as the coordinating moiety in our present "1 to 3" design strategy.

Figure 5 and Table 2 illustrate the in vitro integrin $\alpha_v\beta_3$ binding affinities in cell-binding assays of the metal complexes (Re-[L1] and Re-$[L2]_3$) and the uncomplexed ligands (L1, L2). Re-$[L2]_3$, a trivalent RGD metal complex, displayed an order of magnitude (ca. 8) higher binding affinity than its unlabeled ligand L2 (3.16 vs 25.9 nM), while in the "1 to 1" design, both the metal complex (Re-[L1]) and its unlabeled ligand (L1) showed similar IC_{50} values (38.4 vs 43.3 nM). The enhanced binding affinity of Re-$[L2]_3$ is attributable to the presence of trivalent RGD motif in Re-$[L2]_3$ which is similar in magnitude to trivalent RGD peptides reported previously.[28] This clearly demonstrates that increased binding affinity toward a targeted molecule can be achieved by metal complexation of multiple monovalent ligands such that the metal complex is transformed and acts as a multivalent species.

The biodistribution studies in tumor bearing nude mice were conducted to compare the in vivo targeting potential and pharmacokinetics of the ^{99m}Tc-labeled probes derived from the "1 to 1" design and the in situ multivalent "1 to 3" design (Table 3). Although the postlabeling purification is not compatible with the original purpose in this study, we included the HPLC-purified ^{99m}Tc-labeled probes into the biodistribution studies to elucidate the in vivo behavior of the ^{99m}Tc-labeled probes free from the competitive inhibitions caused by the presence of the unlabeled ligands. The higher tumor uptake of purified ^{99m}Tc-$[L2]_3$ than that of purified ^{99m}Tc-[L1] (7.18 ± 0.60 vs 2.77 ± 0.51%ID/g) is consistent with the results obtained in in vitro binding study where Re-$[L2]_3$ showed higher integrin $\alpha_v\beta_3$ binding affinity than did Re-[L1]. Additionally, the tumor uptake of ^{99m}Tc-$[L2]_3$ was significantly blocked with the co-injection of 5 nmol Re-$[L2]_3$ to 1.80 ± 0.14%ID/g, demonstrating that the accumulation of ^{99m}Tc-$[L2]_3$ in the tumor was indeed integrin$\alpha_v\beta_3$ specific. The biodistribution results of the unpurified ^{99m}Tc-labeled probes, where 5 nmol of the unlabeled ligands were co-injected, represent a practical clinical situation where ^{99m}Tc-labeled probes are administered to subjects without purification. Though the tumor uptake of ^{99m}Tc-$[L2]_3$ was partially blocked by the presence of the unlabeled monovalent ligand, the tumor uptake of this unpurified ^{99m}Tc-$[L2]_3$ was still ca. 3-fold higher than that of unpurified ^{99m}Tc-[L1] and was also higher than that of purified ^{99m}Tc-[L1] (3.80 ± 0.57, 1.14 ± 0.11, and 2.77 ± 0.51%ID/g, respectively), thus demonstrating the enhanced in vivo targeting and localization ability of the "1 to 3" designed ^{99m}Tc-labeled probe compared to the conventional monovalent "1 to 1" designed approach. In vivo SPECT/CT imaging studies similar to the clinical scenario were also conducted in a murine tumor model by injecting the unpurified ^{99m}Tc-labeled probes. Figure 6 depicts the comparative SPECT/CT images obtained in the two approaches and also support the superiority of the "1 to 3" design strategy.

DOI: 10.1021/acs.jmedchem.6b00024
J. Med. Chem. XXXX, XXX, XXX−XXX

In comparing tumor uptake of unpurified ^{99m}Tc-[L2]$_3$ and purified ^{99m}Tc-[L2]$_3$ + Re-[L2]$_3$, it is also worth noting that the purified ^{99m}Tc-[L2]$_3$ + Re-[L2]$_3$ condition acts as a mimic of a scenario of a multivalent "1 to 1" design where the unlabeled ligand is a trivalent RGD and can compete with the ^{99m}Tc-labeled trivalent RGD (Figure 1b). The higher tumor uptake of unpurified ^{99m}Tc-[L2]$_3$ than that of purified ^{99m}Tc-[L2]$_3$ + Re-[L2]$_3$ thereby indirectly demonstrates that the in situ multivalent "1 to 3" design strategy is superior in in vivo targeting potential not only to the monovalent "1 to 1" design strategy (Figure 1a) but also to the multivalent "1 to 1" design strategy (Figure 1b).

While these studies illustrate the potential for this novel "1 to 3" multivalent design to provide higher-affinity imaging probes upon metal complexation, it is with the caveat that the results obtained here are all based on the specific experimental conditions (cell line, animal model, amount of unlabeled ligand, etc.), and the expression level of target proteins[37] and/or the amount of unlabeled ligands[38] can intricately affect the degree of competitive inhibition on the target uptake of such radiolabeled probes. Thus, careful consideration should be taken when this design is expanded or applied to other systems, experimental models, or conditions. Nevertheless, this study for the first time has demonstrated the usefulness and potential of the in situ multivalent strategy for the development of target-specific metal-based radiolabeled probes that exhibit high target uptake despite the presence of unlabeled ligand. Thus, this strategy would enable the preparation of radiolabeled probes of high target uptake without postlabeling purification steps, which may accelerate the practice of molecular imaging by radiolabeled probes in preclinical and/or clinical settings.

CONCLUSION

We have developed an in situ multivalent "1 to 3" design to prepare ^{99m}Tc-labeled trivalent probes from isonitrile-derivatized monovalent ligands without postlabeling purification steps. This design concept would provide a kit formulation for on-site synthesis of target-specific ^{99m}Tc-labeled trivalent probes, which allows the full appreciation of the advantage of the metallic radionuclide. In addition, this design may not only be limited to the isonitrile−[^{99m}Tc(CO)$_3$]$^+$ core combination but may also be applicable to other ligand−metal combinations that form mixed ligand complexes of high in vivo stability. Similarly, as the multivalent effect is a universal phenomenon among many kinds of small molecule−protein interactions, this design could be expanded to a variety of biomolecules for molecular imaging and/or targeted radionuclide therapy.

EXPERIMENTAL SECTION

General. All commercially available chemicals were of analytical grade and were used without further purification. Fmoc-protected amino acids and H-Gly-Trt (2-Cl) resin were purchased from Watanabe Chemical Industries, Ltd. (Hiroshima, Japan). c[R(pdf)-GD(*t*Bu)fK] (**1**) and [Re(CO)$_3$(OH$_2$)$_3$]Br (**10**) were synthesized according to the previous report.[21,39] All other reagents were purchased from Wako Pure Chemical Industries, Ltd. (Tokyo). Technetium-99m as Na^{99m}TcO$_4$ was eluted in saline solution on a daily basis from a ^{99} Mo/^{99m}Tc generator (Ultra-Techne Kow, FUJIFILM RI Pharma Co., LTD., Tokyo). Mass spectrometry was carried out using an AccuTOF LC-plus (JMS-T100LP, JEOL Ltd., Tokyo). ^{1}H NMR spectra was recorded on a JEOL ECS-400 (400 MHz) spectrometer (JEOL Ltd., Tokyo). All compounds tested in inhibition assay, biodistribution study, and SPECT study were prepared in >95% purities as determined by HPLC. Different HPLC systems (1−9) were used for various preparative and analytic studies and are detailed in the Supporting Information.

*Boc-Gly-Gly-OH (**2**).* H-GlyGly-OH (50.0 mg, 0.38 mmol) was dissolved in dioxane/water/1N NaOH$_{aq}$ (760 μL/380 μL/380 μL), and di-*tert*-butyl dicarbonate (92.0 mg, 0.42 mmol) was added to this mixture in an ice bath. The reaction mixture was stirred at room temperature for 1 h, and the solvent was evaporated in vacuo. The residue was dissolved in water and washed with hexane. The pH was adjusted to 2 using 5% aqueous citric acid and extracted with ethyl acetate, and the organic layer was dried over magnesium sulfate. After removing the solvent in vacuo, the residue was purified with silica gel column chromatography (chloroform/methanol/acetic acid =10/1/0.1) to afford compound **2** as a white powder (39.6 mg, 42%). ^{1}H NMR (400 MHz, CD$_3$OD): δ 1.46 (s, 9H, *t*Bu), 3.76 (s, 2H, C*H*$_2$), 3.92 (s, 2H, C*H*$_2$COOH). ESI-MS, *m*/*z*: 255.10 [M + H]$^+$, found 255.10.

*H-Gly-Gly-c(RGDfK) (**3**).* The compound **1** (78.5 mg, 0.086 mmol), **2** (20.0 mg, 0.086 mmol), and HOBt (33.0 mg, 0.216 mmol) was dissolved in DMF (1 mL) and stirred in an ice bath for 10 min. To this stirred mixture, DIC (33 μL, 0.216 mmol) was added dropwise and stirred in an ice bath for 10 min, followed by stirring at room temperature for 2 h. After removing the solvent in vacuo, the residue was redissolved in TFA/TES/water (9 mL/0.5 mL/0.5 mL) and stirred at room temperature for 3 h. The solvent was evaporated in vacuo, and diethyl ether was added to form the precipitate. The precipitate was washed with diethyl ether 3 times, purified by preparative HPLC using system 5, and lyophilized to obtain compound **3** as a white powder (2 steps, 36.2 mg, 58.5%). ESI-MS, *m*/*z*: 718.36 [M + H]$^+$, found 718.33.

*Formylamino-β-alanine-OH (**4**).* β-alanine (5.00 g, 56.2 mmol) was dissolved in formic acid/acetic anhydrate (25 mL/13 mL) and stirred at 95 °C under N$_2$ atmosphere for 3 h. After the solvent was evaporated in vacuo, the residue was purified with silica gel column chromatography (chloroform/methanol = 5/1) to afford compound **4** as a white powder (3.97 g, 60.1%). ^{1}H NMR (400 MHz, D$_2$O): δ 2.43 (t, 2H, C*H*$_2$CO), 3.30 (t, 2H, NHC*H*$_2$), 7.83 (s, 1H, formylamino). ESI-MS, *m*/*z*: 118.05 [M + H]$^+$, found 118.09.

*2,3,5,6-Tetrafluorophenyl Formylamino-β-alanine (**5**).* **4** (1.00 g, 7.6 mmol) and TFP (1.39 g, 8.4 mmol) were dissolved in DMF (10 mL) and stirred in an ice bath for 10 min. To this stirred mixture, DCC (1.72 g, 8.4 mmol) was added and stirred in an ice bath for 10 min, followed by stirring at room temperature overnight. After removing dicyclohexylurea by filtration, the solvent was removed in vacuo and purified with silica gel column chromatography (ethyl acetate) to afford compound **5** as a white powder (1.21 g, 53%). ^{1}H NMR (400 MHz, CDCl$_3$): δ 2.95 (t, 2H, C*H*$_2$CO), 3.68 (q, 2H, NHC*H*$_2$), 6.25 (br, 1H, NH), 7.00 (m, 1H, H$_{arom}$), 8.17 (s, 1H, formylamino). ESI-MS, *m*/*z*: 266.04 [M + H]$^+$, found 266.04.

*2,3,5,6-Tetrafluorophenyl isocyano-β-alanine (**6**).* The compound **5** (0.30 g, 1.1 mmol) and Burgess reagent (0.26 g, 1.1 mmol) were dissolved in dichloromethane (10 mL) and stirred at 50 °C for 3 h. After removing the solvent in vacuo, the residue was purified with silica gel chromatography (chloroform/acetonitrile = 3/1) to afford compound **6** as a white powder (0.23 g, 83.1%). ^{1}H NMR (400 MHz, CDCl$_3$): δ 3.11 (t, 2H, C*H*$_2$CO), 3.81 (t, 2H, NC*H*$_2$), 7.02 (m, 1H, H$_{arom}$). ^{13}C NMR (100 MHz, CDCl$_3$): δ 33.37 (s, CH$_2$CO), 36.71 (t, NCH$_2$), 103.74 (t, C$_{arom}$H), 128−147 (multiple peaks, C$_{arom}$F), 158.61 (s, CN), 165.58 (s, CO).

*CN-βAla-GG-RGD (L2) (**7**).* The compound **3** (9.6 mg, 13.4 μmol) and DIPEA (3.4 μL, 20 μmol) were dissolved in DMF (200 μL) and stirred in an ice bath for 10 min. The compound **6** (4.0 mg, 16 μmol) was added to this mixture and stirred at room temperature for 1 h. The precipitate formed upon addition of diethyl ether was collected, purified with preparative HPLC using system 3, and lyophilized to obtain compound **7** as a white powder (5.2 mg, 49%). The >95% purities were determined by HPLC using system 9 (Figure S2). ESI-MS, *m*/*z*: 799.39 [M + H]$^+$, found 799.44.

*L-Cysteine, S-(2-carboxyethyl)-N-(tert-butoxycarbonyl), 1-methyl ester (**8**).* *N*-(tert-butoxycarbonyl)-L-cysteine methyl ester (117.7 mg, 0.5 mmol) and DIPEA (350 μL, 2 mmol) were dissolved in DMF (150

DOI: 10.1021/acs.jmedchem.6b00024
J. Med. Chem. XXXX, XXX, XXX−XXX

μL) and stirred in an ice bath for 10 min. To this stirred mixture, 3-iodo-propionic acid (100 mg, 0.5 mmol) dissolved in DMF (150 μL) was added and stirred in an ice bath for 10 min, followed by stirring at room temperature for 3 h. After removing the solvent in vacuo, the residue was purified with silica gel column chromatography (chloroform/methanol/acetic acid = 30/1/0.1) to afford compound **8** as a pale yellow powder (93.8 mg, 61%). ^{1}H NMR (400 MHz, $CDCl_3$): δ 1.45 (s, 9H, *t*Bu), 2.64 (t, 2H, CH_2CO), 2.80 (t, 2H, SCH_2), 3.00 (br, 2H, CH_2S), 3.77 (s, 3H, OCH_3), 4.54 (br, 1H, α-proton). ESI-MS, *m*/*z*: 330.10 $[M + Na]^+$, found 330.09.

*3-L-Cysteine Propionic Acid-c(RGDfK), 1-Methyl Ester (L1) (**9**).* The compound **1** (21 mg, 0.023 mmol), **8** (7.8 mg, 0.025 mmol), and HOBt (8.44 mg, 0.063 mmol) were dissolved in DMF (200 μL) and stirred in an ice bath for 10 min. To this stirred mixture, DIC (8.8 μL, 0.063 mmol) was added and stirred in an ice bath for 10 min, followed by stirring at room temperature for 1 h. After removing the solvent in vacuo, the residue was redissolved in TFA/TES/water (9 mL/0.5 mL/0.5 mL) and stirred at room temperature for 3 h. The solvent was evaporated in vacuo, and diethyl ether was added to form the precipitate. The precipitate was washed with diethyl ether 3 times, purified by preparative HPLC using system 4, and lyophilized to obtain compound **9** as a white powder (2 steps, 3.6 mg, 18%). The >95% purities were determined by HPLC using system 6 (Figure S4). ESI-MS, *m*/*z*: 793.37 $[M + H]^+$, found 793.39.

*$[Re(CO)_3(L2)_3]^+$ (Re-[L2]$_3$) (**11**).* The rhenium compound **10** (0.683 mg, 1.69 μmol) and **7** (L2, 13.5 mg, 16.9 μmol) were dissolved in 0.1 M A.B. (pH 6.0, 1 mL). The mixture was heated at 90 °C for 3 h and purified by preparative HPLC using system 1. The fractions containing the desired product were collected and lyophilized to obtain compound **11** as a white powder (4.1 mg, 90%). The >95% purities were determined by HPLC using system 6 (Figure S3). ESI-MS, *m*/*z*: 1334.04 $[M + H]^{2+}$, found 1334.41

*$[Re(CO)_3(L1)]$ (Re-[L1]) (**12**).* The rhenium compound **10** (3.77 mg, 9.33 μmol) and L1 (7.4 mg, 9.33 μmol) were dissolved in 0.1 M A.B. (pH 6.0, 1 mL). The mixture was heated at 70 °C for 3 h and purified by preparative HPLC using system 2. The fractions containing the desired product were collected and lyophilized to obtain compound **12** as a white powder (2.3 mg, 23.5%). The >95% purities were determined by HPLC using system 7 (Figure S5). ESI-MS, *m*/*z*: 1049.28 $[M + H]^+$, found 1049.49.

$[^{99m}Tc(CO)_3(OH_2)_3]^+$. $[^{99m}Tc(CO)_3(OH_2)_3]^+$ was prepared according to a reported method with slight modifications.[26] Briefly, a kit containing 0.285 mg sodium tetraborate decahydrate ($Na_2B_4O_7 \cdot 10H_2O$), 0.715 mg sodium carbonate (Na_2CO_3), 1 mg sodium (+)-tartrate dihydrate ($C_4H_4Na_2O_6 \cdot 2H_2O$), and 0.45 mg sodium boranocarbonate $[Na_2(H_3BCO_2)]$ was purged with N_2 atmosphere before adding 300 μL $^{99m}TcO_4^-$ (111 MBq) to a sealed vial. The mixture was heated for 7 min at 100 °C, and the pH was adjusted to 6 with 1 N HCl_{aq}. The purities were determined by radio-HPLC using system 6.

Preparation of ^{99m}Tc-[L2]$_3$. A 100 μL (37 MBq) solution of freshly prepared $[^{99m}Tc(CO)_3(OH_2)_3]^+$ was added to a vial containing 165 μL (0.1 M A.B., pH 6.0) of L2 solution to reach the final ligand concentration of 150 μM (40 nmol/265 μL). The mixture was then heated at 110 °C for 20 min, followed by 100 °C for 20 min under N_2 atmosphere in a heating block. The radiochemical purities were determined by radio-HPLC using system 6.

Preparation of ^{99m}Tc-[L1]. A 150 μL (55.5 MBq) solution of freshly prepared $[^{99m}Tc(CO)_3(OH_2)_3]^+$ was added to a vial containing 250 μL (0.1 M A.B., pH 6.0) of L1 solution to reach the final ligand concentration of 50 μM (20 nmol/400 μL). The mixture was heated at 110 °C for 30 min under N_2 atmosphere in a heating block. The radiochemical purities were determined by radio-HPLC using system 7.

Determination of Log $D_{7.4}$ Values. ^{99m}Tc-[L1] and ^{99m}Tc-[L2]$_3$ were purified by HPLC (systems 7 and 6, respectively), and the eluents of the two compounds were evaporated in vacuo. Then, the residues were dissolved in 25 mM phosphate buffer (pH 7.4) to prepare 3.7 MBq/mL sample solutions. Ten μL (37 kBq) of each sample solution was added to an equal volume mixture (3 mL:3 mL) of *n*-octanol and 25 mM phosphate buffer (pH 7.4) pre-incubated for 24 h to reach equilibrium. The mixtures were vortexed for 1 min, followed by being left to stand for 1 min. This procedure was repeated 3 times. The mixtures were then centrifuged at 3000 rpm for 5 min. The samples from both *n*-octanol and aqueous layers were obtained and counted in an autowell γ counter. The log $D_{7.4}$ values were reported as mean ± SD of 3 experiments.

Stability Assessment. The unlabeled ligand in ^{99m}Tc-[L2]$_3$ was removed by the HPLC using system 6. The radioactive peak was collected, and the solvent was removed in vacuo. The residue was reconstituted in 0.001% v/v TritonX-100 in D-PBS (−), and 10 μL of the ^{99m}Tc-[L2]$_3$ solution was mixed with 190 μL of histidine solution to reach the final histidine concentration of 10 mM. Similarly 10 μL of this ^{99m}Tc-[L2]$_3$ solution was mixed with 190 μL of freshly prepared murine plasma. After incubation at 37 °C for 1 and 6 h, 1 μL of aliquots were drawn and analyzed with radio-TLC (n = 3) (Silica gel 60 F_{254}, Merck Ltd., Tokyo) developed with MeOH:10% w/w $AcONH_4$ in water = 1:1. For HPLC analysis of the histidine sample, the incubation solution was directly analyzed by radio-HPLC using system 6. For HPLC analysis of the plasma sample, 200 μL of EtOH was added to 100 μL of the plasma incubate to precipitate the proteins. The sample was centrifuged at 15,000 *g* for 5 min at 4 °C. The supernatant was collected, and the pellet was washed with 300 μL of 66% v/v EtOH in D-PBS(−) and centrifuged. This washing step was repeated twice. The supernatants of both centrifugation steps were combined and analyzed by HPLC using system 6. The recovery rate of radioactivity from the plasma sample was determined by following equation, (the radioactivity of the supernatant)/(the original radioactivity of the plasma sample) × 100 (n = 3). The radioactivity was determined using an autowell γ counter (WIZARD 1480, PerkinElmer Japan Co., Ltd., Yokohama, Japan).

Binding Affinity to Integrin $\alpha_v\beta_3$. U87MG human glioma cells were grown in Dulbecco's modified eagle medium (Sigma-Aldrich Japan K.K., Tokyo) supplemented with 10% v/v fetal bovine serum (Nippon Biosupply Center, Tokyo) and 1% v/v penicillin-streptomycin (10,000 unit-10 mg/mL, Sigma-Aldrich Japan K.K.) at 37 °C in humidified atmosphere containing 5% CO_2. Multiscreen DV filter plates (Merck Millipore, MA) were seeded with 2×10^5 cells in the binding buffer (20 mM Tris, 150 mM NaCl, 2 mM $CaCl_2$, 1 mM $MgCl_2$, 1 mM $MnCl_2$, 0.1% BSA, pH 7.4), and the mixtures were incubated at 37 °C with ^{125}I-c(RGDyV) in the presence of increasing concentrations of c(RGDyV), L1, Re-[L1], L2, or Re-[L2]$_3$. The total incubation volume was adjusted to 200 μL. After incubatation for 1 h at 37 °C, the plates were filtered and washed twice with 200 μL of the ice-cold binding buffer. The polyvinylidene fluoride filters were collected, and the radioactivity was determined using an autowell γ counter. The IC_{50} values were calculated by fitting the data by nonlinear regression using GraphPad Prism (GraphPad Software, Inc., San Diego, CA). All the binding experiments were carried out with quadruplet samples.

Animal Model. Animal studies were conducted in accordance with the institutional guidelines approved by the Chiba University Animal Care Committee. BALBc nu/nu male mice (Japan SLC, Inc., Shizuoka, Japan) 6 weeks old were xenografted by subcutaneous injection of U87MG human glioblastoma cells (5×10^6 cells/50 μL of culture medium) into their right hind legs. The mice were subjected to biodistibution studies as well as SPECT/CT imaging studies when the tumor weight reached 0.1−0.5 g.

Biodistribution. Male nude mice bearing tumor xenografts of U87MG were injected via the tail vein with 100 μL (11.1 kBq) of ^{99m}Tc-[L1] (L1 = 5 nmol) as the monovalent "1 to 1" design, ^{99m}Tc-[L2]$_3$ (Re-[L2]$_3$ = 5 nmol) as the multivalent "1 to 1" design, or ^{99m}Tc-[L2]$_3$ (L2 = 5 nmol) as the "1 to 3" design. In case of multivalent "1 to 1" design, Re-[L2]$_3$ was added to the HPLC-purified ^{99m}Tc-[L2]$_3$ solution. In addition, HPLC-purified ^{99m}Tc-[L1] and ^{99m}Tc-[L2]$_3$ were also evaluated using similar methods. The animals were sacrificed and dissected at 1 h after administration. The tissues of interest were removed and weighed, and the radioactivity was determined with an autowell gamma counter. The results are

DOI: 10.1021/acs.jmedchem.6b00024
J. Med. Chem. XXXX, XXX, XXX−XXX

presented as the percentage injected dose per gram (%ID/g) or percentage injected dose per tissue (%ID). Values were expressed as mean ± SD for a group of 5 animals.

Small Animal SPECT/CT Imaging Study. SPECT images were acquired over 45−75 min after intravenous administration of ^{99m}Tc-[L1] (100 μL, 9.6 MBq, L1 = 5 nmol) or ^{99m}Tc-[L2]$_3$ (100 μL, 7.4 MBq, L2 = 5 nmol) to male BALBc nu/nu mice bearing U87MG xenografts via the tail vein. CT scans were performed before SPECT scans for anatomic reference. The mice were anaesthetized with 1−2% (v/v) isoflurane (DS Pharma Animal Health, Osaka, Japan) and positioned on the animal bed where anesthesia was continuously delivered via a nose cone system. SPECT imaging and X-ray CT imaging were performed by use of small animal SPECT/CT system (Triumph LabSPECT4/CT, TriFoil Imaging Inc., Chatsworth, CA) equipped with a five pinhole (0.5 mm) collimator. Data acquisition was performed for 30 min at 30 s per projection with stepwise rotation of 60 projections over 360°.

■ ASSOCIATED CONTENT

Supporting Information

The Supporting Information is available free of charge on the ACS Publications website at DOI: 10.1021/acs.jmedchem.6b00024.

HPLC methods, HPLC chromatograms of ^{99m}Tc-[L1] and Re-[L1], purity checks and characterizations of the compounds **7**, **9**, **11**, **12**, and ^{1}H NMR and/or ^{13}C NMR of the compounds **4**-**6** (PDF)

■ AUTHOR INFORMATION

Corresponding Author

*Phone: +81-43-226-2896. E-mail: arano@chiba-u.jp. Fax: +81-43-226-2897.

Notes

The authors declare no competing financial interest.

■ ACKNOWLEDGMENTS

This work was supported in part by the Grants-in-Aids for the Development of Systems and Technology for Advanced Measurement and Analysis Program (Development of SPECT probe for molecular imaging) from Japan Science and Technology Agency, JST, and JSPS Research Fellows Program (no. 264896).

■ ABBREVIATIONS USED

A.B., acetate buffer; Boc, *tert*-butoxycarbonyl; *t*Bu, *tert*-butyl; DIC, *N*,*N*′-diisopropylcarbodiimide; DIPEA, *N*,*N*-diisopropylethylamine; DMF, *N*,*N*-dimethylformamide; HOBt, 1-hydroxybenzotriazole; TES, triethylsilane; TFA, trifluoroacetic acid; TFP, 2,3,5,6-tetrafluoro phenol; pbf, 2,2,4,6,7-pentamethyldihydrobenzofuran-5-sulfonyl

■ REFERENCES

(1) Gambhir, S. S. Molecular imaging of cancer with positron emission tomography. *Nat. Rev. Cancer* **2002**, *2*, 683−693.

(2) Ametamey, S. M.; Honer, M.; Schubiger, P. A. Molecular imaging with PET. *Chem. Rev.* **2008**, *108*, 1501−1516.

(3) Herschman, H. R. Molecular imaging: Looking at problems, seeing solutions. *Science* **2003**, *302*, 605−608.

(4) Rahmim, A.; Zaidi, H. PET versus SPECT: strengths, limitations and challenges. *Nucl. Med. Commun.* **2008**, *29*, 193−207.

(5) Meikle, S. R.; Kench, P.; Kassiou, M.; Banati, R. B. Small animal SPECT and its place in the matrix of molecular imaging technologies. *Phys. Med. Biol.* **2005**, *50*, R45−R61.

(6) Liu, S.; Edwards, D. S. ^{99m}Tc-labeled small peptides as diagnostic radiopharmaceuticals. *Chem. Rev.* **1999**, *99*, 2235−2268.

(7) Liu, S. Bifunctional coupling agents for radiolabeling of biomolecules and target-specific delivery of metallic radionuclides. *Adv. Drug Delivery Rev.* **2008**, *60*, 1347−1370.

(8) Bartholomae, M. D.; Louie, A. S.; Valliant, J. F.; Zubieta, J. Technetium and gallium derived radiopharmaceuticals: comparing and contrasting the chemistry of two important radiometals for the molecular imaging era. *Chem. Rev.* **2010**, *110*, 2903−2920.

(9) Bhattacharyya, S.; Dixit, M. Metallic radionuclides in the development of diagnostic and therapeutic radiopharmaceuticals. *Dalton Trans.* **2011**, *40*, 6112−6128.

(10) Liu, S.; Chakraborty, S. ^{99m}Tc-centered one-pot synthesis for preparation of ^{99m}Tc radiotracers. *Dalton Trans.* **2011**, *40*, 6077−6086.

(11) Arano, Y. Recent advances in ^{99m}Tc radio pharmaceuticals. *Ann. Nucl. Med.* **2002**, *16*, 79−93.

(12) Eckelman, W. C. Radiolabeling with technetium-99m to study high-capacity and low-capacity biochemical systems. *Eur. J. Nucl. Med.* **1995**, *22*, 249−263.

(13) Kung, M. P.; Stevenson, D. A.; Plossl, K.; Meegalla, S. K.; Beckwith, A.; Essman, W. D.; Mu, M.; Lucki, I.; Kung, H. F. [^{99m}Tc]TRODAT-1: A novel technetium-99m complex as a dopamine transporter imaging agent. *Eur. J. Nucl. Med.* **1997**, *24*, 372−380.

(14) Ballinger, J. R. The influence of carrier on ^{99m}Tc radiopharmaceuticals. *Q. J. Nucl. Med.* **2002**, *46*, 224−232.

(15) Oxboel, J.; Brandt-Larsen, M.; Schjoeth-Eskesen, C.; Myschetzky, R.; El-Ali, H. H.; Madsen, J.; Kjaer, A. Comparison of two new angiogenesis PET tracers ^{68}Ga-NODAGA-E[c(RGDyK)]$_2$ and ^{64}Cu-NODAGA-E[c(RGDyK)]$_2$; in vivo imaging studies in human xenograft tumors. *Nucl. Med. Biol.* **2014**, *41*, 259−267.

(16) Kiessling, L. L.; Gestwicki, J. E.; Strong, L. E. Synthetic multivalent ligands in the exploration of cell-surface interactions. *Curr. Opin. Chem. Biol.* **2000**, *4*, 696−703.

(17) Mammen, M.; Choi, S. K.; Whitesides, G. M. Polyvalent interactions in biological systems: Implications for design and use of multivalent ligands and inhibitors. *Angew. Chem., Int. Ed.* **1998**, *37*, 2754−2794.

(18) Chen, X.; Guo, Y.; Zhang, Q.; Hao, G.; Jia, H.; Liu, B. Preparation and biological evaluation of ^{99m}Tc-CO-MIBI as myocardial perfusion imaging agent. *J. Organomet. Chem.* **2008**, *693*, 1822−1828.

(19) Hao, G.; Zang, J.; Liu, B. Preparation and biodistribution of novel ^{99m}Tc(CO)$_3$-CNR complexes for myocardial imaging. *J. Labelled Compd. Radiopharm.* **2007**, *50*, 13−18.

(20) Hao, G. Y.; Zang, J. Y.; Zhu, L.; Guo, Y. Z.; Liu, B. L. Synthesis, separation and biodistribution of ^{99m}Tc-CO-MIBI complex. *J. Labelled Compd. Radiopharm.* **2004**, *47*, 513−521.

(21) Haubner, R.; Wester, H. J.; Reuning, U.; Senekowitsch-Schmidtke, R.; Diefenbach, B.; Kessler, H.; Stöcklin, G.; Schwaiger, M. Radiolabeled $\alpha_v\beta_3$ integrin antagonists: A new class of tracers for tumor targeting. *J. Nucl. Med.* **1999**, *40*, 1061−1071.

(22) Shi, J.; Wang, L.; Kim, Y. S.; Zhai, S.; Liu, Z.; Chen, X.; Liu, S. Improving tumor uptake and excretion kinetics of ^{99m}Tc-labeled cyclic arginine-glycine-aspartic (RGD) dimers with triglycine linkers. *J. Med. Chem.* **2008**, *51*, 7980−7990.

(23) Wang, L.; Shi, J.; Kim, Y. S.; Zhai, S.; Jia, B.; Zhao, H.; Liu, Z.; Wang, F.; Chen, X.; Liu, S. Improving tumor-targeting capability and pharmacokinetics of ^{99m}Tc-Labeled cyclic RGD dimers with PEG$_4$ linkers. *Mol. Pharmaceutics* **2009**, *6*, 231−245.

(24) Psimadas, D.; Fani, M.; Gourni, E.; Loudos, G.; Xanthopoulos, S.; Zikos, C.; Bouziotis, P.; Varvarigou, A. D. Synthesis and comparative assessment of a labeled RGD peptide bearing two different ^{99m}Tc-tricarbonyl chelators for potential use as targeted radiopharmaceutical. *Bioorg. Med. Chem.* **2012**, *20*, 2549−2557.

(25) Creedon, S. M.; Crowley, H. K.; McCarthy, D. G. Dehydration of formamides using the Burgess Reagent: A new route to isocyanides. *J. Chem. Soc., Perkin Trans. 1* **1998**, 1015−1017.

(26) Alberto, R.; Ortner, K.; Wheatley, N.; Schibli, R.; Schubiger, A. P. Synthesis and properties of boranocarbonate: A convenient in situ

DOI: 10.1021/acs.jmedchem.6b00024
J. Med. Chem. XXXX, XXX, XXX−XXX

CO source for the aqueous preparation of $[^{99m}Tc(OH_2)_3(CO)_3]^+$. *J. Am. Chem. Soc.* **2001**, *123*, 3135−3136.
(27) Chakraborty, S.; Shi, J.; Kim, Y. S.; Zhou, Y.; Jia, B.; Wang, F.; Liu, S. Evaluation of ^{111}In-labeled cyclic RGD peptides: Tetrameric not tetravalent. *Bioconjugate Chem.* **2010**, *21*, 969−978.
(28) Notni, J.; Pohle, K.; Wester, H. J. Be spoilt for choice with radiolabelled RGD peptides: Preclinical evaluation of ^{68}Ga-TRAP-$(RGD)_3$. *Nucl. Med. Biol.* **2013**, *40*, 33−41.
(29) Janssen, M. L.; Oyen, W. J.; Dijkgraaf, I.; Massuger, L. F.; Frielink, C.; Edwards, D. S.; Rajopadhye, M.; Boonstra, H.; Corstens, F. H.; Boerman, O. C. Tumor targeting with radiolabeled $\alpha_v\beta_3$ integrin binding peptides in a nude mouse model. *Cancer Res.* **2002**, *62*, 6146−6151.
(30) Lindner, S.; Michler, C.; Wängler, B.; Bartenstein, P.; Fischer, G.; Schirrmacher, R.; Wängler, C. PESIN multimerization improves receptor avidities and in vivo tumor targeting properties to GRPR-overexpressing tumors. *Bioconjugate Chem.* **2014**, *25*, 489−500.
(31) Dong, C.; Zhao, H.; Yang, S.; Shi, J.; Huang, J.; Cui, L.; Zhong, L.; Jin, X.; Li, F.; Liu, Z.; Jia, B.; Wang, F. ^{99m}Tc-labeled dimeric octreotide peptide: A radiotracer with high tumor uptake for single-photon emission computed tomography imaging of somatostatin receptor subtype 2-positive tumors. *Mol. Pharmaceutics* **2013**, *10*, 2925−2933.
(32) Banerjee, S. R.; Pullambhatla, M.; Shallal, H.; Lisok, A.; Mease, R. C.; Pomper, M. G. A modular strategy to prepare multivalent inhibitors of prostate-specific membrane antigen (PSMA). *Oncotarget* **2011**, *2*, 1244−1253.
(33) Yanagi, M.; Uehara, T.; Uchida, Y.; Kiyota, S.; Kinoshita, M.; Higaki, Y.; Akizawa, H.; Hanaoka, H.; Arano, Y. Chemical design of ^{99m}Tc-labeled probes for targeting osteogenic bone region. *Bioconjugate Chem.* **2013**, *24*, 1248−1255.
(34) Oliveira, B. L.; Morais, M.; Mendes, F.; Moreira, I. S.; Cordeiro, C.; Fernandes, P. A.; Ramos, M. J.; Alberto, R.; Santos, I.; Correia, J. D. Re(I) and Tc(I) complexes for targeting nitric oxide synthase: Influence of the chelator in the affinity for the enzyme. *Chem. Biol. Drug Des.* **2015**, *86*, 1072−1086.
(35) Schibli, R.; La Bella, R.; Alberto, R.; Garcia-Garayoa, E.; Ortner, K.; Abram, U.; Schubiger, P. A. Influence of the denticity of ligand systems on the in vitro and in vivo behavior of ^{99m}Tc(I)-tricarbonyl complexes: A hint for the future functionalization of biomolecules. *Bioconjugate Chem.* **2000**, *11*, 345−351.
(36) Kurz, P.; Spingler, B.; Fox, T.; Alberto, R. $[Tc^1(CN)_3(CO)_3]^{2-}$ and $[Re^1(CN)_3(CO)_3]^{2-}$: Case studies for the binding properties of CN- and CO. *Inorg. Chem.* **2004**, *43*, 3789−3791.
(37) Tolmachev, V.; Wållberg, H.; Sandström, M.; Hansson, M.; Wennborg, A.; Orlova, A. optimal specific radioactivity of anti-HER2 affibody molecules enables discrimination between xenografts with high and low HER2 expression levels. *Eur. J. Nucl. Med. Mol. Imaging* **2011**, *38*, 531−539.
(38) Tolmachev, V.; Rosik, D.; Wallberg, H.; Sjoberg, A.; Sandstrom, M.; Hansson, M.; Wennborg, A.; Orlova, A. Imaging of EGFR expression in murine xenografts using site-specifically labelled anti-EGFR ^{111}In-DOTA-$Z_{EGFR:2377}$ affibody molecule: Aspect of the injected tracer amount. *Eur. J. Nucl. Med. Mol. Imaging* **2010**, *37*, 613−622.
(39) Lazarova, N.; James, S.; Babich, J.; Zubieta, J. A convenient synthesis, chemical characterization and reactivity of $[Re(CO)_3(H_2O)_3]Br$: The crystal and molecular structure of $[Re(CO)_3(CH_3CN)_2Br]$. *Inorg. Chem. Commun.* **2004**, *7*, 1023−1026.

DOI: 10.1021/acs.jmedchem.6b00024
J. Med. Chem. XXXX, XXX, XXX−XXX